Elastic energy and interactions between twin boundaries in nanotwinned gold

Yen Fred Woguem, Pierre Godard, J. Durinck, Sandrine Brochard

Elastic energy and interactions between twin boundaries in nanotwinned gold

Yen Fred Woguem*, Pierre Godard, Julien Durinck, Sandrine Brochard

Université de Poitiers, ISAE-ENSMA, CNRS, PPRIME, Poitiers, France

Abstract

Nanotwinned metals exhibit a surprising combination of ultrahigh strength and high ductility. We have performed atomistic simulations in gold to study interactions between coherent twin boundaries (CTBs) and between incoherent twin boundaries (ITBs) for two extreme cases: with close surfaces and without any surface, in order to simulate a relaxed or a constrained system. The estimated displacement fields give the extension of interactions between twin boundaries which are 6 atomic planes for the CTB and in the range of 30-42 atomic planes for the $\Sigma3\{112\}$ ITB in the relaxed system. The displacement field in the constrained system is, to a very good approximation, the difference of the displacement field in the relaxed system and a homogeneous quantity which depends on the excess volumes. The elastic strain introduced by the twin boundaries in the constrained system and the associated elastic energy γ_{excess} are deduced from the excess volumes. Our study highlights how the mechanical behaviour (e.g. the yield strength) of samples with TBs separated by distances less thana critical distance whose order of magnitude is $(10^3 - 10^5)\ \delta_{TB} \approx (0.5 - 360)$ nm can be affected.

Keywords: Molecular statics, Excess volume, Twin boundary, Elastic energy, Gold

Introduction

Defects play a key role in the properties of materials. This is the case for twin boundaries (TBs) which improve mechanical properties without degrading the electrical conductivity [1, 2]. The energy and structure of symmetric and asymmetric $\Sigma3$ grain boundaries have been investigated, and it has been shown that local energy minima correspond to symmetric configurations with $\{111\}$, $\{112\}$ and $\{110\}$ boundary planes. Hence arbitrary $\Sigma3$ asymmetric grain boundaries tend to facet into $\Sigma3\{111\}$ coherent twin boundaries (CTBs), $\Sigma3\{112\}$ incoherent twin boundaries (ITBs) and $\Sigma3\{110\}$ incoherent twin boundaries which have also been observed in some cases [3, 4, 5, 6, 7, 8, 9, 10]. This justifies in depth studies of $\Sigma3\{111\}$ CTBs and $\Sigma3\{112\}$ ITBs. These two TBs have been observed experimentally using transmission electron microscopy [11, 12, 13, 14, 15]. Atomic scale simulations have been used to study the interactions of $\Sigma3\{111\}$ CTBs with other types of crystal defects such as vacancies, interstitials [16], stacking fault tetrahedra [17], and dislocations [18, 19, 20, 21]. Some experimental and simulation studies have shown that the TB junctions $\{111\}||\{11\bar{2}\}||\{111\}$ are not stable because they can migrate, which is accomplished by the detwinning of CTBs during annealing [13, 12, 22], under a shear stress [23] or under irradiation [24, 25].

The study of the interaction energy between two CTBs for two materials, aluminium (Al) and copper (Cu), has shown that it is attractive [13]. Other studies for gold and other metals have shown that the interaction between two CTBs is limited to six layers between the CTBs [26, 27, 28]. TBs interact via the atomic displacements that each one generates. The excess volume being the sum of the atomic displacements along the normal to the TB, its value corresponds to the expansion or contraction that the TB introduces in the system. When the system is constrained, an elastic field counterbalances this expansion or contraction, and this introduces an additional energy term. It has been shown in the literature that the yield strength of twinned gold or copper nanowires of finite length during deformation is affected by the distance between coherent twin boundaries (CTBs) [2, 29, 30]. Some explanations have been given for this effect on the mechanical properties in nanotwinned materials. However, the contribution of the elastic energy induced by the excess volumes of the TBs has not been considered.

We had recourse to molecular static (MS) simulations to characterize the elastic displacement field created by one TB and study the interaction between TBs. Three interatomic potentials commonly encountered in the literature for gold have been compared. We have also determined the elastic energy induced by the TBs when the system is constrained, and used the results to discuss the ensuing effect in nanotwinned materials. This paper is organized as follows: the model and methods are detailed in section 1, the results are presented in section 2 and discussed in section 3.

*Corresponding author, email address: yen.fred.woguem@univ-poitiers.fr

1. Model and Methods

For this study, we considered $\Sigma3\{111\}$ CTBs and, independently, $\Sigma3\{112\}$ ITBs in a face-centred cubic (fcc) crystal. Both TBs can be constructed by tilt operations: the CTB by cutting the crystal along a (111) plane and performing a 180° rotation of one part around the $[11\bar{2}]$ direction, and the ITB by cutting the crystal along a $(11\bar{2})$ plane and performing a 180° rotation of one part around the [111] direction (figure 1.a).

The computational cell was built by repeating n_u, n_v and n_w times the 6 atom fcc unit cell along the basis vectors $\vec{u} = a_0[111]$, $\vec{v} = \frac{a_0}{2}[1\bar{1}0]$ and $\vec{w} = \frac{a_0}{2}[11\bar{2}]$, respectively, with a_0 the lattice parameter of the Au single crystal. For the ITB configuration, the normal to the twin boundary is along $\vec{w}$ and the size of the simulation cell is such that $n_u = 6$ and $n_v = 12$. For the CTB configuration, the normal to the twin boundary is along $\vec{u}$ and the size of the simulation cell is such that $n_v = 24$ and $n_w = 4$. In the following, several distances between free surfaces and/or twin boundaries were considered by taking variable values for n_w and n_u in ITB and CTB configurations, respectively. We have considered multiples of three and six planes respectively for distances between CTBs and between ITBs because they correspond to the stacking period along the directions normal to the TBs. We have used MS calculations with LAMMPS (Large-Scale Atomic Molecular Massively Parallel Simulator) [33]. The Embedded-Atom Method (EAM) interatomic potentials of Foiles [34] and Grochola [35], and Modified Embedded-Atom Method (MEAM) interatomic potential of Baskes [36] as implemented by Lee et al [37] have been used. Some characteristics of gold fcc phase for the three potentials are given and compared to experimental data in table 1. The relaxation of the ITB leads to the formation of the 9R phase [11, 12, 13, 38], as illustrated in figure 1.b for Foiles potential. The ABC stacking sequence of {111} planes in an fcc phase becomes ABCBCACAB in the 9R phase. This 9R phase can also be described using hexagonal (H) and fcc (C) planes with the CHHCHHCHH sequence. For Grochola and Baskes potentials, a portion of 9R phase is also obtained, as presented and discussed in [39]. The main difference between the three potentials is the width of the 9R phase: the larger width is obtained for the Foiles potential, and the smallest for the Baskes potential. Relaxation of the model was done using the Hessian-free truncated Newton algorithm at 0 K. All atom positions are relaxed fully and independently until all the force components on any atom do not exceed 10^{-4} eV/Å. The analyses of the obtained structures have been performed with the OVITO (Open Visualization Tool) software [40].

2. Results

2.1. Interactions between twin boundaries in a fully relaxed system

We have first studied the interaction between two twin boundaries with free surfaces along the z direction (the normal to the TBs) while periodic boundary conditions (PBC) are imposed in all other directions. The normalized energy introduced by the TBs in the system has been determined from MS with the formula

$$\gamma_{TB}^{(2)} = \frac{E_{tot} - E_0}{2 \times S} \tag{1a}$$

where E_{tot} is the total energy of the relaxed system with the two TBs, E_0 is the energy of the relaxed reference system (system with only surfaces) with the same number of atoms and S is the surface of one TB. The energy $\gamma_{TB}^{(2)}$ can be separated into several terms:

$$\gamma_{TB}^{(2)} = \gamma_{TB} + \frac{\gamma_{TB-TB}^{(i)}}{2} + \gamma_{TB-surfaces}^{(i)} \tag{1b}$$

where γ_{TB} is the energy of an isolated TB, $\gamma_{TB-TB}^{(i)}$ is the interaction energy between the two TBs and $\gamma_{TB-surfaces}^{(i)}$ is the interaction between one TB and the surfaces. We have checked that the distances between the TBs and the surfaces were large enough for this last contribution to be neglected. To do so, we first constructed a system with a single twin boundary and two surfaces to study the TB-surface interaction. The curve giving the interaction energy as a function of the TB-surface distance allowed us to determine the distance where the interaction is negligible. We choose this TB-surface distance (or larger) in the system with two twin boundaries and two surfaces to study the TB-TB interaction without the effect of the TB-surface interaction. The energy γ_{TB} and the excess volume δ_{TB} of an isolated TB have been calculated in a previous work [39]. The results are given in table 1. We recall that the excess volume is defined as the variation of volume per unit area of twin boundary (which is related to the atomic displacement created by the TB).

Figures 2.a and 2.b show the interaction energy $\gamma_{TB-TB}^{(i)}$ between two TBs for the Foiles, Baskes and Grochola potentials obtained with equation (1b) in which $\gamma_{TB-surfaces}^{(i)}$ can be neglected as mentioned above. $\gamma_{TB}^{(2)}$ and γ_{TB} are obtained from our MS calculations (equation (1a) and table 1). We observe that the interaction energy between the two CTBs is attractive for the three potentials (figure 2.a), which is in good agreement with the results shown in the literature for Cu and Al [13]. Above 15 Å $\sim$ 6 atomic planes the interaction energy becomes negligible for the three potentials, or more precisely $\gamma_{CTB-CTB}^{(i)} \,/\, \gamma_{CTB} < 10^{-4}$ for those distances (table 2). This is in compliance with the results found in the literature [26, 27, 28]. For the ITB, the interaction energy between two ITBs is attractive for the Baskes potential but

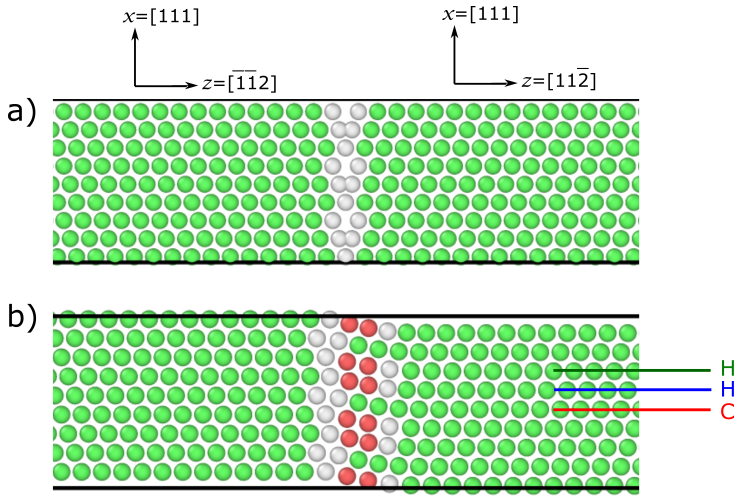

Figure 1: a) Unrelaxed and b) relaxed {112} ITB atomic structures obtained with the Foiles potential. Atoms are colored according to the common neighbour analysis (CNA) parameter (characteristic of the local crystal structure around an atom [31, 32]): atoms in an fcc, a hexagonal and an unidentified crystal arrangement are respectively in green, red and white. The green, blue and red lines correspond respectively to the H, H and C planes of figure 2.

	Foiles	Baskes	Grochola	Experiment
γ_{ISF} (mJ/m^2)	4.8	56	42.6	33 [41]
a_0 (Å)	4.08	4.07	4.07	4.08 [42]
C_{zz} (GPa) (along $\langle 111 \rangle$ direction)	224	225	241	241 [43]
C_{zz} (GPa) (along $\langle 112 \rangle$ direction)	213	216	231	231 [43]
γ_{CTB} (mJ/m^2)	2.4	20.2	21.3	/
γ_{ITB} (mJ/m^2)	386.9	438.3	371.1	/
δ_{CTB} (Å)	-1.2×10^{-3}	2.9×10^{-3}	-2.0×10^{-3}	/
δ_{ITB} (Å)	0.02	0.06	-0.002	/

Table 1: Fcc gold intrinsic stacking fault energy γ_{ISF}, lattice parameter a_0, stiffness coefficients along $\langle 111 \rangle$ and $\langle 112 \rangle$ directions, energy and excess volume of TBs obtained for the three potentials and corresponding experimental data when available.

		Foiles	Baskes	Grochola
Distance (Å)	CTB	15	15	15
	ITB	30	35	25
Atomic planes	CTB	6	6	6
	ITB	36	42	30

Table 2: Critical distances (for the three potentials) for which the interaction energy between the two TBs satisfies $\gamma^{(i)}_{TB-TB} \,/\, \gamma_{TB} < 10^{-4}$.

slightly repulsive for the Foiles and Grochola potentials. Above the critical distance mentioned in table 2 the interaction energy becomes negligible for the three potentials using the same criterion as for the CTB. When the interaction energy is non negligible (for the smaller distances), the interaction energy between the CTBs is much smaller than the one between the ITBs (e.g. at a TB-TB distance of 20 Å for the Baskes potential $\gamma^{(i)}_{ITB-ITB} \simeq 10^6 \times \gamma^{(i)}_{CTB-CTB}$), except for the Grochola potential for which the interaction energy between CTBs is quite the same than the one between the ITBs. We note that there is no correlation between the sign of δ_{TB} and the character (repulsive or attractive) of the TB-TB interaction.

To account for the elastic displacement field created by one TB, we computed the interplanar spacing variation $\Delta d_i^{(relax)}$ with respect to the bulk equilibrium value (d_e). $\Delta d_i^{(relax)}$ versus the position along the normal to the TB is shown in figures 2.c-2.f. For the ITB, we consider both the C and the two H planes. For the three potentials, the elastic displacement field induced by the CTB is limited to around 10 Å, that is $\Delta d_i^{(relax)}/d_e < 10^{-4}$ wherever the atoms are more than 8 Å apart from the CTB; for the ITB (for the three planes C, H and H) the elastic displacement field extends between 20 and 23 Å with the same criterion. Of course, there is a correlation between the interaction energy range of TBs and the elastic displacement field: when the elastic displacement field increases, the interaction energy between TBs increases, and when the elastic displacement field generated by the TBs becomes negligible, the interaction energy becomes negligible. For the same TBs, the interaction energy is different for each potential because of the different elastic displacement fields. Finally, we note that, though the elastic displacement field extension is of the same order of magnitude for the two TBs, its maximum value is around 100 times larger for ITBs than for CTBs.

2.2. Interactions between twin boundaries in a constrained system

In this part, the studied system is the same as the previous one, except that the free surfaces along z have been replaced by PBC. To simulate a constrained system, the atomic positions have been relaxed without relaxation of the simulation cell (figure 3). The size of the system L_z along the z direction is twice the distance between TBs. The normalized energy introduced by the TBs has been calculated from MS with the formula

$$\gamma^{(\infty)}_{TB} = \frac{E_{tot} - E_0}{2 \times S} \tag{2a}$$

where E_{tot} is the energy of the system with the two TBs, E_0 is the energy of the reference system (without TB) and S is the surface of each TB. The symbol ∞ means that there is an infinity of TBs because of the PBC. The energy $\gamma^{(\infty)}_{TB}$ can be separated into several terms:

$$\gamma^{(\infty)}_{TB} = \gamma_{TB} + \frac{\gamma^{(i)(\infty)}_{TB-TB}}{2} + \gamma_{excess} \tag{2b}$$

with $\gamma^{(i)(\infty)}_{TB-TB}$ the interaction energy between one TB and all its TBs neighbors in the system (the other TB in the simulation cell and all the images produced by the PBC) and γ_{excess} the elastic energy ensuing from the excess volume in the system.

The energy $\gamma^{(\infty)}_{TB} - \gamma_{TB}$ in the simulation cell containing two TBs and with PBC is presented in figure 4 as a function of the distance between TBs. According to equation (2b), the variation of this energy is due to the interaction between TBs and to the elastic energy γ_{excess}. We observe that, for the three potentials and the two types of TBs, this function decreases when the distance between TBs increases. When the distance between TBs is large, $\gamma^{(i)(\infty)}_{TB-TB}$ and γ_{excess} become negligible, since $\gamma^{(\infty)}_{TB}$ converges to the energy γ_{TB} of a single TB in a relaxed system (table 1). We focus in the following of this work on the elastic energy γ_{excess} to evaluate its contribution in equation (2b).

To deepen our understanding of γ_{excess}, we computed the interplanar spacing variation $\Delta d_i^{(const)}$ along the TBs in the constrained systems. As shown for the CTB in figure 5 for 48 atomic planes in the system, $\Delta d_i^{(const)}$ is very well approximated by the difference of the corresponding variation in a relaxed system, $\Delta d_i^{(relax)}$, and of a homogeneous quantity, which appears to be $4\delta_{TB} d_e/L_z$: $\Delta d_i^{(const)} \approx \Delta d_i^{(relax)} - 4\delta_{TB} d_e/L_z$. Using the values of δ_{CTB}, d_e and L_z for each potential (table 1), the homogeneous quantities are respectively -1.0×10^{-4} for the Foiles potential, 2.5×10^{-4} Å for the Baskes potential and -1.7×10^{-4} for the Grochola potential which are in good agreement with the values given by the simulations in figure 5 for the CTB. In other words, the excess volume is homogeneously distributed over the entire length of the system. Hence, the elastic energy γ_{excess} generated by a TB in a constrained system can be explicitly modeled. The elastic strain necessary to go from a relaxed system (with length $L_z + 4\delta_{TB}$ along z) to the constrained system (with length L_z) in a system with two TBs (see figure 3) is

$$\varepsilon_{zz} = \frac{-4\delta_{TB}}{L_z + 4\delta_{TB}}. \tag{3}$$

This strain is homogeneous in the whole system as explained above. We consider that $\varepsilon_{ij} = 0$ for $i, j \neq z$; hence,

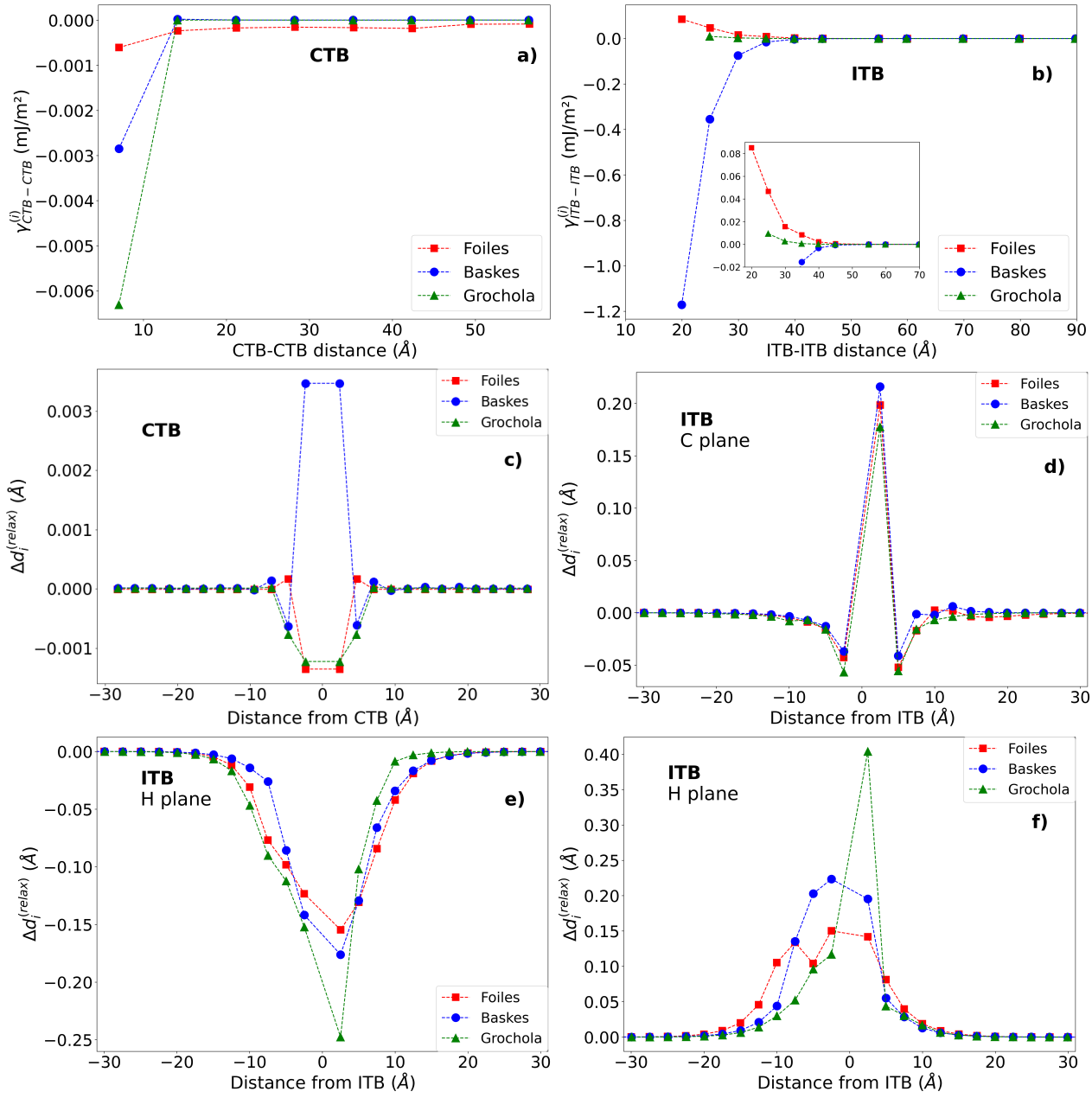

Figure 2: Interaction energy between two a) CTBs and b) ITBs as a function of the distance between the TBs (the inset shows zoom-in of the curves for the three potentials). c), d), e) and f) represent the difference ($\Delta d_i^{(relax)}$) between the interplanar spacing in the system with one TB and the interplanar spacing d_e in the bulk system versus the distance along the normal to the TB respectively for the system containing a CTB and for three planes of the system containing an ITB (CHH).

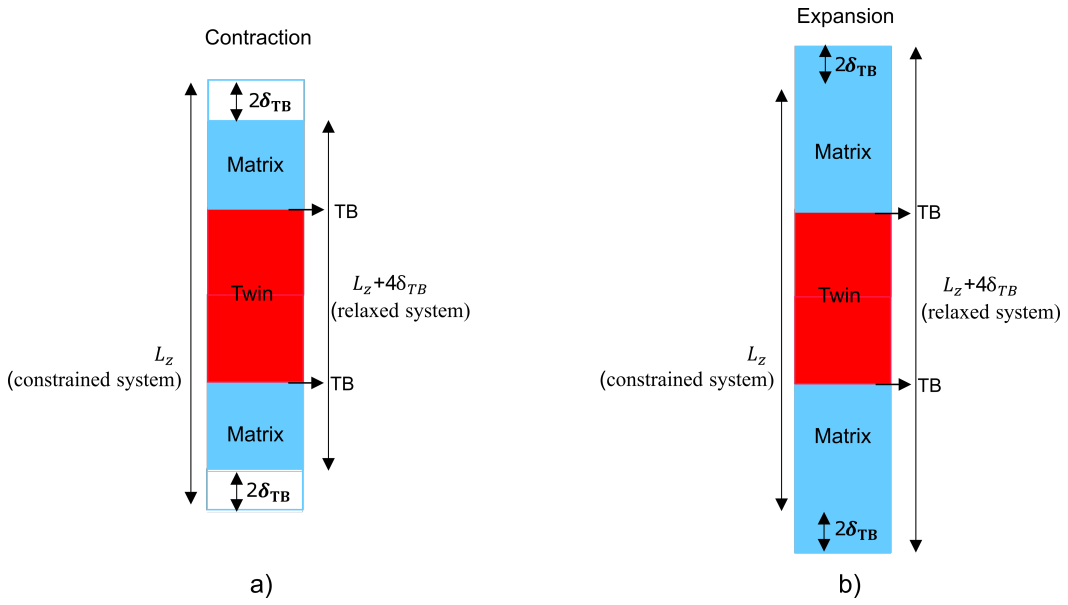

Figure 3: Constrained and relaxed systems with two TBs. a) Contraction ($\delta_{TB} < 0$) or b) expansion ($\delta_{TB} > 0$) introduced by the excess volume $4\delta_{TB}$ for two TBs in the crystal.

according to this model, the elastic energy $2S\gamma_{excess}^{(model)}$ is:

$$2S\gamma_{excess}^{(model)} = \frac{V}{2}\sigma_{zz}\varepsilon_{zz}, \tag{4a}$$

$$2S\gamma_{excess}^{(model)} = \frac{S}{2}C_{zz}\frac{16\delta_{TB}^2 L_z}{(L_z+4\delta_{TB})^2} \tag{4b}$$

where $V = L_z S$ is the volume of the crystal, C_{zz} the stiffness coefficient along the direction normal to the TB so that $\sigma_{zz} = C_{zz}\varepsilon_{zz}$. We deduce that the energy of the model is given by

$$\gamma_{excess}^{(model)} = 4C_{zz}\delta_{TB}^2\frac{L_z}{(L_z+4\delta_{TB})^2}. \tag{5}$$

The results obtained with the simulations (symbols) and with the model (continuous line) for CTBs and ITBs are represented in figure 4. In the system studied with our MS simulations L_z is twice the distance between TBs. The model is in very good agreement with the simulation results for both types of TBs and for the three potentials. This means that the elastic energy γ_{excess} has a major contribution in equation (2b) compared to the TBs interaction energy. More quantitatively, the TBs interaction energy can be evaluated by the difference between the simulated results and the analytical model of excess energy: this shows that the order of magnitude of the interactions between TBs is the same for both constrained and unconstrained systems. Moreover, we point out that the stiffness coefficients and excess volumes used in the model are not fitted values but they are obtained with atomistic simulations (table 1).

3. Discussion

Now we are going to discuss about the elastic energy γ_{excess} ensuing from the excess volume in the system between TBs and between potentials. We will also discuss the parameters on which this elastic energy depends.

For Foiles and Baskes potentials, the elastic energy γ_{excess} is larger for the ITBs than for the CTBs. For the Grochola potential it is almost the same for the two TBs. For the CTB, the larger elastic energy γ_{excess} is obtained for the Baskes potential, and the smallest elastic energy γ_{excess} is obtained for the Foiles potential, while for the ITB, the larger elastic energy γ_{excess} is obtained for the Baskes potential, and the smallest elastic energy γ_{excess} is obtained for the Grochola potential. It becomes negligible for the critical distance L_z^* between TBs given by

$$L_z^* = \frac{4C_{zz}\delta_{TB}^2}{10^{-4}\gamma_{TB}}, \tag{6}$$

for which $\gamma_{excess}/\gamma_{TB} < 10^{-4}$ and considering that $L_z + 4 \times \delta_{TB} \approx L_z$ (because $L_z \geq 14$ Å and the maximum value of $4 \times \delta_{TB}$ is 0.24 Å). The critical distance L_z^* was determined for the two types of TB and the three potentials using the model, and the results are presented in table 3. The order of magnitude of the critical distance is $(10^3 - 10^5)\delta_{TB} \simeq (0.5 - 360)$ nm.

The model (equation (5)) highlights that the elastic energy γ_{excess} depends on the excess volume generated by the TB and the elastic constants along the normal to the TB. To explain the difference of the elastic energy γ_{excess} between the three potentials and between the two TBs, we have computed the variation of the elastic energy

		Foiles	Grochola	Baskes
Distance (Å)	CTB	260	100	200
	ITB	450	5	3550
$\frac{Distance}{\lvert\delta_{TB}\rvert}$	CTB	2.17×10^5	5.00×10^4	6.90×10^4
	ITB	2.25×10^4	2.50×10^3	5.92×10^4

Table 3: Critical distances between TBs and for different potentials, for which elastic energy is negligible ($\gamma_{excess}/\gamma_{TB} < 10^{-4}$), and ratio between the critical distance and excess volume.

TBs	CTB	ITB
$\frac{\Delta C_{zz}}{C_{zz}^{max}}$	7.1% (Foiles/Grochola)	7.8% (Foiles/Grochola)
$\frac{\Delta\lvert\delta_{TB}\rvert}{\lvert\delta_{TB}\rvert^{max}}$	59% (Foiles/Baskes)	97% (Grochola/Baskes)

Table 4: Relative variation of elastic constants and excess volume between the three potentials for each TBs. ΔC_{zz} or $\Delta|\delta|$ are the variations between the maximum and the minimum values of the three potentials , C_{zz}^{max} and $|\delta_{TB}|^{max}$ are respectively the maximum values of C_{zz} and $|\delta_{TB}|$ between the three potentials.

Potential	Foiles	Baskes	Grochola
$\frac{\Delta C_{zz}}{C_{zz}^{max}}$ (CTB/ITB)	5%	4%	4%
$\frac{\Delta\lvert\delta_{TB}\rvert}{\lvert\delta_{TB}\rvert^{max}}$ (CTB/ITB)	94%	95%	0%

Table 5: Relative variation of elastic constants and excess volume between both TBs for each potential. C_{zz}^{max} and $|\delta_{TB}|^{max}$ are respectively the maximum values of C_{zz} and $|\delta_{TB}|$ between the two TBs.

$\frac{\Delta\gamma_{excess}}{\gamma_{excess}}$. According to equation (5):

$$\frac{\Delta\gamma_{excess}}{\gamma_{excess}} = \frac{\Delta C_{zz}}{C_{zz}} + 2 \times \frac{\Delta|\delta_{TB}|}{|\delta_{TB}|}. \quad (7)$$

where once again it is considered that $L_z + 4 \times \delta_{TB} \approx L_z$.

We have computed $\frac{\Delta C_{zz}}{C_{zz}^{max}}$ and $\frac{\Delta|\delta_{TB}|}{|\delta_{TB}|^{max}}$ using the values given in table 1. The results are displayed in tables 4 and 5. It is clear from table 4 that the main contribution to the variation of the elastic energy γ_{excess} between the three potentials comes from the variation of the excess volume whatever the TB types. Indeed, the variation of elastic constants ($\frac{\Delta C_{zz}}{C_{zz}^{max}}$) is always small compared to that of the excess volume ($\frac{\Delta|\delta_{TB}|}{|\delta_{TB}|^{max}}$) (less than 8% compared to more than 50%).

Table 5 shows that for Foiles and Baskes potentials the main contribution to the variation of the elastic energy γ_{excess} between the two TB types also comes from the variation of the excess volume. Here again, the variation of elastic constants ($\frac{\Delta C_{zz}}{C_{zz}^{max}}$) is always small compared to that of the excess volume ($\frac{\Delta|\delta_{TB}|}{|\delta_{TB}|^{max}}$) (less than 6% compared to more than 90%).

The small contribution of the elastic constant variations $\frac{\Delta C_{zz}}{C_{zz}}$ results from the fact that the potentials are adjusted so as to give reliable elastic constants; hence, these weakly depend on the potential. Moreover, it appears that the C_{zz} values are similar whether z corresponds to a $< 111 >$ or $< 112 >$ direction. On the contrary, the predicted excess volume values greatly depend on the potential and, except for the Grochola potential, on the TB type (table 1).

As a result, the higher values of the elastic energy γ_{excess} for the Baskes potential ensue from the higher values of the excess volume (for example there is a factor of 30 between δ_{ITB} for the Baskes potential and δ_{ITB} for the Grochola potential, which explains the higher values obtained for the Baskes potential in figure 4.b). Similarly the elastic energy γ_{excess} is larger for ITBs than for CTBs because ITBs have a greater value of excess volume than CTBs ($|\ \delta_{ITB}\ | \approx 10 \times |\ \delta_{CTB}\ |$), except for the Grochola potential for which the elastic energy γ_{excess} is the same for both TBs because they have the same excess volume value.

In this work, we considered three different well-known and reliable interatomic potentials for gold, already used in the literature in particular for the study of twinning or twinned nanowires [29, 44, 45, 46]. As shown in table 1, the excess volumes obtained with the different potentials are significantly different, both in sign and in amplitude, whether it is for the CTB or for the ITB. Furthermore, these variations do not appear to be related to those of specific properties related to twinning or twin boundaries: there is no obvious correlation between the intrinsic stacking fault energies or the TBs energies and the excess volumes (table 1). So these energetic quantities can not be used within our model for predictions, for which a direct measure of the excess volumes would be better. But if it is possible to determine experimentally the elastic constants, the measure of the excess volume, though not impossible [47], is difficult, making it tricky to assess its contribution. Another option in order to rationalize the results and to compare e.g. different materials would be to use ab initio calculations to obtain accurate values of the excess volumes. Although a detailed study of this type is beyond

the scope of the present article, a first insight into such an analysis can be given with the outcomes of [39]. They indicate that for gold, the most accurate potential, as far as excess volumes are concerned, would be the MEAM Baskes potential, although the Grochola potential shows better intrinsic stacking fault energy when compared to experimental or ab initio values.

Our study focusing on two extreme cases can help to understand the different mechanical behaviours of samples with TBs whose distances are less than a critical distance whose order of magnitude is $(10^3 - 10^5)\ \delta_{TB} \simeq (0.5 - 360)$ nm. Indeed, for constrained systems, the TBs will generate important residual stresses (related to the elastic energy γ_{excess}) which can affect the mechanical properties of the material, whereas the average residual stresses vanish in relaxed systems. We emphasize that it is not easy to determine the detailed stress state in a real system. The completely constrained system considered in this paper is an extreme case which may be seen as a textbook case, and it gives an upper bound on the stress lying in some systems and its consequences on, e.g., the yield strength.

Among the systems for which the excess volume may not be fully relaxed, we can cite for example the 4 μm thick polycrystalline copper samples of [2], where the average distance between CTBs is 15 nm and the 1-2 μm thick polycrystalline silver samples of [48], where the average distance between CTBs may be as small as 3.6 nm. These examples concern twins with CTBs parallel to the surface; the constrain is probably larger when the twins are inclined, as in [49] or [50], where the CTB-CTB distance is 5-10 nm. Finally, the excess volume relaxation may also be impeded when the twins do not come from the elaboration process but result from deformation, as in the cyclic tests of [51], where nanotwin formation was presumed to assist grain coarsening. We note that these last examples concern gold, with CTBs and ITBs.

Conclusion

In summary, we have studied a relaxed and a constrained system.

In the relaxed system we have studied the interaction energy between $\Sigma3\{111\}$ CTBs and between $\Sigma3\{112\}$ ITBs using MS with three potentials. The interaction energy between CTBs is attractive for the three potentials. For the ITBs this interaction is repulsive for Foiles and Grochola potentials while it is attractive for the Baskes potential. Our study shows how the intensity of the interaction energy between TBs is related to the elastic displacement field. The interaction energy between CTBs has a lower extension than the one for ITBs, and this is correlated to the elastic displacement field induced by each TB.

In the constrained system, we have studied the elastic energy generated by the TBs. We suggest a decomposition into two terms, $\gamma^{(i)(\infty)}_{TB-TB}$ and γ_{excess}, the latter ensuing only from the excess volume created by the TBs. γ_{excess} is explicitly computed, and, for the two types of TBs and for the three potentials, its values dominate over $\gamma^{(i)(\infty)}_{TB-TB}$. The extension of this elastic energy is limited to a critical distance L_z whose order of magnitude is $(10^3 - 10^5)\ \delta_{TB} \approx (0.5 - 360)$ nm. The difference between the elastic energy created by CTBs and ITBs, and between the three potentials is mainly related to the excess volume.

This work highlights how the mechanical behaviour (e.g. the yield strength) of samples with TBs separated by distances less than a critical distance whose order of magnitude is $(10^3 - 10^5)\ \delta_{TB} \approx (0.5 - 360)$ nm can be affected.

This works was funded by the French National Research Agency, grant reference ANR-19-CE08-0007. This work also pertains to the the France 2030 program "Investissements d'Avenir" (LABEX INTERACTIFS, reference ANR-11-LABX-0017-01) and to the French Government program "Investissements d'Avenir" EUR INTREE, reference ANR-18-EURE-0010.

References

[1] L. Lu, Y. Shen, X. Chen, L. Qian, K. Lu, Ultrahigh strength and high electrical conductivity in copper, Science 304 (2004) 422–426. doi:10.1126/science.1092905.
URL https://www.science.org/doi/abs/10.1126/science.1092905

[2] L. Lu, X. Chen, X. Huang, K. Lu, Revealing the maximum strength in nanotwinned copper, Science 323 (5914) (2009) 607–610. doi:10.1126/science.1167641.
URL https://www.science.org/doi/abs/10.1126/science.1167641

[3] U. Wolf, F. Ernst, T. Muschik, M. W. Finnis, H. F. Fischmeister, The influence of grain boundary inclination on the structure and energy of $\sum$3 grain boundaries in copper, Philos. Mag. A 66 (1992) 991–1016. doi:10.1080/01418619208248003.
URL https://doi.org/10.1080/01418619208248003

[4] M. Sennour, S. Lartigue-Korinek, Y. Champion, M. J. Hÿtch†, HRTEM study of defects in twin boundaries of ultra-fine grained copper, Philos. Mag. 87 (2007) 1465–1486. doi:10.1080/14786430601021611.
URL https://doi.org/10.1080/14786430601021611

[5] M. A. Tschopp, D. L. McDowell, Asymmetric tilt grain boundary structure and energy in copper and aluminium, Philos. Mag. 87 (2007) 3147–3173. doi:10.1080/14786430701255895.
URL https://doi.org/10.1080/14786430701255895

[6] J. Wang, N. Li, A. Misra, Structure and stability of $\sum$ 3 grain boundaries in face centered cubic metals, Philos. Mag. 93 (2013) 315–327. doi:10.1080/14786435.2012.716908.
URL https://doi.org/10.1080/14786435.2012.716908

[7] A. D. Banadaki, S. Patala, A simple faceting model for the interfacial and cleavage energies of $\sum$3 grain boundaries in the complete boundary plane orientation space, Comput. Mater. Sci. 112 (2016) 147–160. doi:10.1016/j.commatsci.2015.09.062.
URL https://www.sciencedirect.com/science/article/pii/S0927025615006436

[8] A. Hallil, A. Metsue, J. Bouhattate, X. Feaugas, Correlation between vacancy formation and $\sum$3 grain boundary structures in nickel from atomistic simulations, Philos. Mag. 96 (2016) 2088–2114. doi:10.1080/14786435.2016.1189616.
URL https://doi.org/10.1080/14786435.2016.1189616

[9] J. Humberson, E. A. Holm, Anti-thermal mobility in the $\sum$3 [111] 60° {11 8 5} grain boundary in nickel: Mechanism and computational considerations, Scr. Mater. 130 (2017) 1–6. doi:10.1016/j.scriptamat.2016.10.032.
URL https://www.sciencedirect.com/science/article/pii/S1359646216305279

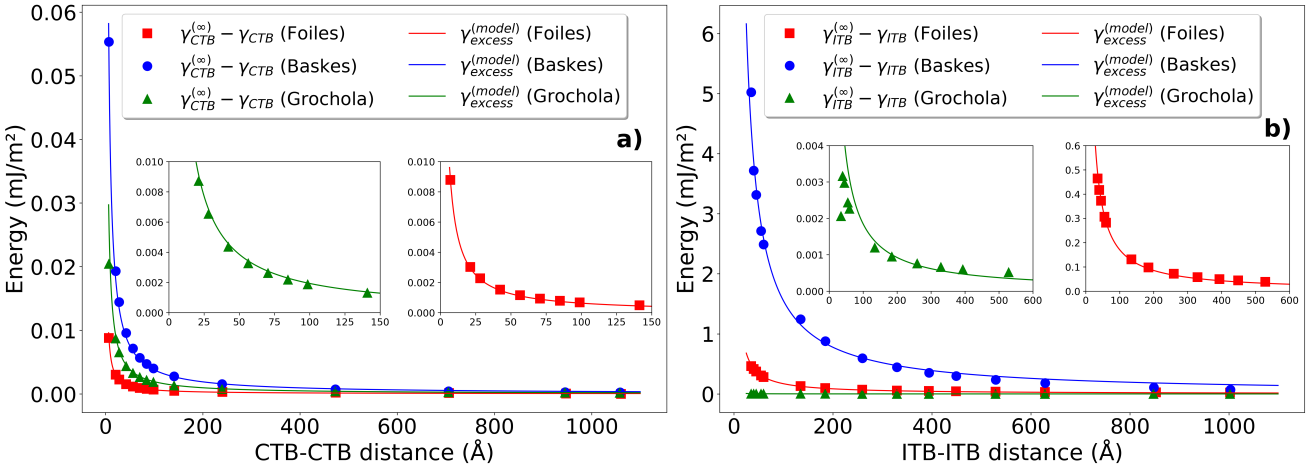

Figure 4: Square, round and triangle symbols: energy $\gamma_{TB}^{(\infty)} - \gamma_{TB}$ (see equation (2b)) in the system with PBC (constrained) for respectively Foiles, Baskes and Grochola potentials for a) CTB and b) ITB as a function of the distance between the TB. The continuous lines represent the elastic model (equation (5)). The insets show zoom-in of the curves for Foiles and Grochola potentials.

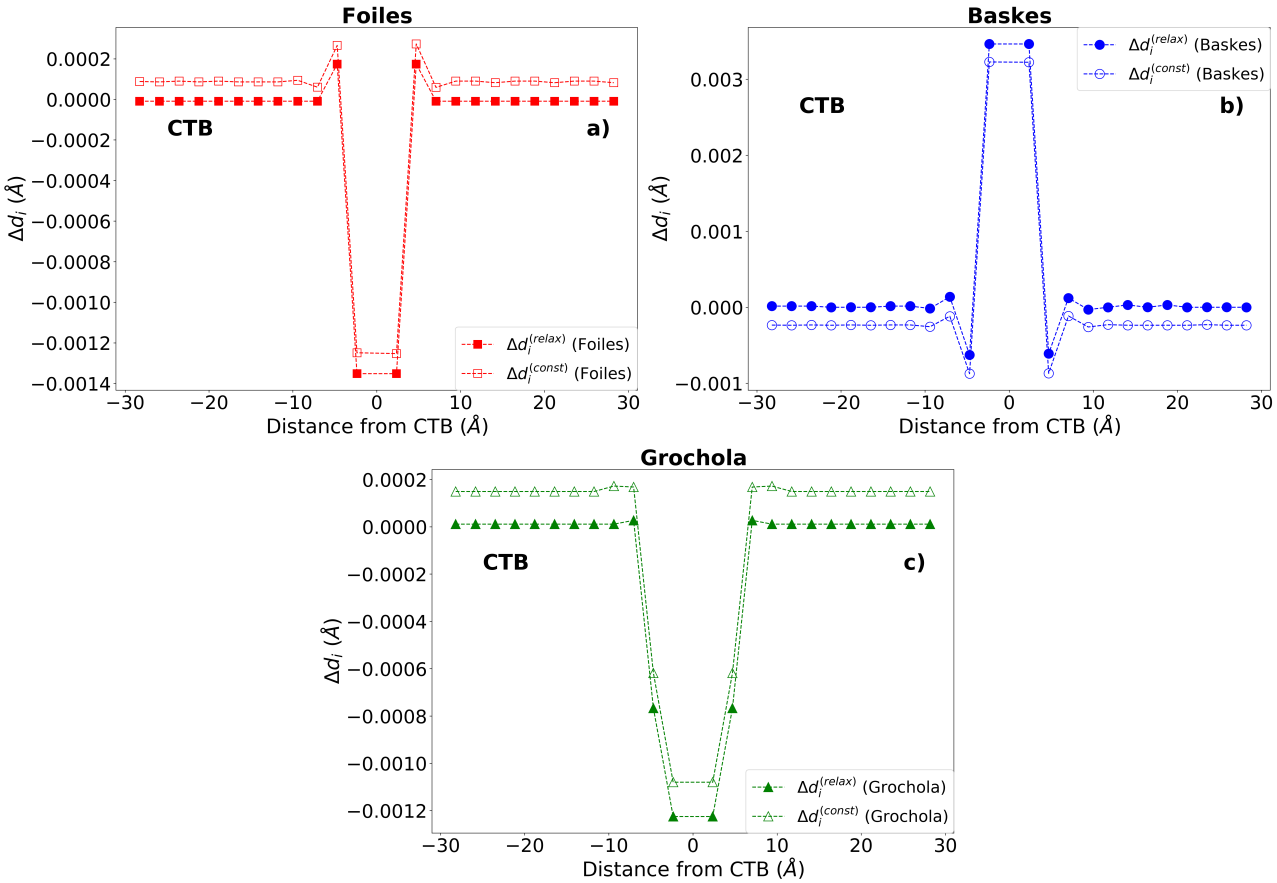

Figure 5: Difference (Δd_i) between the interplanar spacing in the system with a CTB and the interplanar spacing d_e in the bulk system for both relaxed and constrained systems and for the three potentials, versus the distance along the normal to the CTB. Full and empty symbols represent respectively the relaxed ($\Delta d_i^{(relax)}$) and the constrained ($\Delta d_i^{(const)}$) systems. The system length is $n_u = 16$ (113 Å).

[10] J. Humberson, I. Chesser, E. A. Holm, Contrasting thermal behaviors in $\sum 3$ grain boundary motion in nickel, Acta Mater. 175 (2019) 55–65. doi:10.1016/j.actamat.2019.06.003.
URL https://www.sciencedirect.com/science/article/pii/S1359645419303623

[11] D. L. Medlin, G. H. Campbell, C. B. Carter, Stacking defects in the 9R phase at an incoherent twin boundary in copper, Acta Mater. 46 (1998) 5135–5142. doi:10.1016/S1359-6454(98)00164-5.
URL https://www.sciencedirect.com/science/article/pii/S1359645498001645

[12] L. Xu, D. Xu, K. N. Tu, Y. Cai, N. Wang, P. Dixit, J. H. L. Pang, J. Miao, Structure and migration of (112) step on (111) twin boundaries in nanocrystalline copper, J. Appl. Phys. 104 (2008) 113717. doi:10.1063/1.3035944.
URL https://aip.scitation.org/doi/abs/10.1063/1.3035944

[13] J. Wang, N. Li, O. Anderoglu, X. Zhang, A. Misra, J. Y. Huang, J. P. Hirth, Detwinning mechanisms for growth twins in face-centered cubic metals, Acta Mater. 58 (2010) 2262–2270. doi:10.1016/j.actamat.2009.12.013.
URL https://www.sciencedirect.com/science/article/pii/S1359645409008556

[14] L. Liu, J. Wang, S. K. Gong, S. X. Mao, High resolution transmission electron microscope observation of zero-strain deformation twinning mechanisms in Ag, Phys. Rev. Lett. 106 (2011) 175504. doi:10.1103/PhysRevLett.106.175504.
URL https://link.aps.org/doi/10.1103/PhysRevLett.106.175504

[15] N. Lu, K. Du, L. Lu, H. Q. Ye, Motion of $1/3\langle 111\rangle$ dislocations on $\sum 3$ $\{112\}$ twin boundaries in nanotwinned copper, J. Appl. Phys. 115 (2014) 024310. doi:10.1063/1.4861868.
URL https://aip.scitation.org/doi/abs/10.1063/1.4861868

[16] M. J. Demkowicz, O. Anderoglu, X. Zhang, A. Misra, The influence of $\sum 3$ twin boundaries on the formation of radiation-induced defect clusters in nanotwinned Cu, J. Mater. Res. 26 (2011) 1666–1675. doi:10.1557/jmr.2011.56.
URL https://doi.org/10.1557/jmr.2011.56

[17] M. Niewczas, R. Hoagland, Molecular dynamic studies of the interaction of $a/6\langle 112\rangle$ shockley dislocations with stacking fault tetrahedra in copper. part II: Intersection of stacking fault tetrahedra by moving twin boundaries, Philos. Mag. 89 (2009) 727–746. doi:10.1080/14786430902740703.
URL https://doi.org/10.1080/14786430902740703

[18] Z. H. Jin, P. Gumbsch, K. Albe, E. Ma, K. Lu, H. Gleiter, H. Hahn, Interactions between non-screw lattice dislocations and coherent twin boundaries in face-centered cubic metals, Acta Mater. 56 (2008) 1126–1135. doi:10.1016/j.actamat.2007.11.020.
URL https://www.sciencedirect.com/science/article/pii/S1359645407007768

[19] C. Deng, F. Sansoz, Repulsive force of twin boundary on curved dislocations and its role on the yielding of twinned nanowires, Scripta Materialia 63 (1) (2010) 50–53. doi:10.1016/j.scriptamat.2010.03.005.
URL https://www.sciencedirect.com/science/article/pii/S1359646210001430

[20] E. Martínez, B. P. Uberuaga, I. J. Beyerlein, Interaction of small mobile stacking fault tetrahedra with free surfaces, dislocations, and interfaces in Cu and Cu-Nb, Phys. Rev. B 93 (2016) 054105. doi:10.1103/PhysRevB.93.054105.
URL https://link.aps.org/doi/10.1103/PhysRevB.93.054105

[21] Q. Fang, F. Sansoz, Influence of intrinsic kink-like defects on screw dislocation – coherent twin boundary interactions in copper, Acta Mater. 123 (2017) 383–393. doi:10.1016/j.actamat.2016.10.032.
URL https://www.sciencedirect.com/science/article/pii/S1359645416307996

[22] J. A. Brown, N. M. Ghoniem, Structure and motion of junctions between coherent and incoherent twin boundaries in copper, Acta Mater. 57 (2009) 4454–4462. doi:10.1016/j.actamat.2009.06.009.
URL https://www.sciencedirect.com/science/article/pii/S1359645409003474

[23] M. Winning, In-situ observations of coupled grain boundary motion, Philos. Mag. 87 (2007) 5017–5031. doi:10.1080/14786430701601759.
URL https://doi.org/10.1080/14786430701601759

[24] K. Y. Yu, D. Bufford, C. Sun, Y. Liu, H. Wang, M. A. Kirk, M. Li, X. Zhang, Removal of stacking-fault tetrahedra by twin boundaries in nanotwinned metals, Nat. Commun. 4 (1) (2013) 1377. doi:10.1038/ncomms2382.
URL https://www.nature.com/articles/ncomms2382

[25] N. Li, J. Wang, Y. Q. Wang, Y. Serruys, M. Nastasi, A. Misra, Incoherent twin boundary migration induced by ion irradiation in Cu, J. Appl. Phys. 113 (2013) 023508. doi:10.1063/1.4774242.
URL https://aip.scitation.org/doi/abs/10.1063/1.4774242

[26] A. Goyal, Y. Li, A. Chernatynskiy, J. S. Jayashankar, M. C. Kautzky, S. B. Sinnott, S. R. Phillpot, The influence of alloying on the stacking fault energy of gold from density functional theory calculations, Comput. Mater. Sci. 188 (2021) 110236. doi:10.1016/j.commatsci.2020.110236.
URL https://www.sciencedirect.com/science/article/pii/S0927025620307278

[27] H. Gholizadeh, C. Draxl, P. Puschnig, The influence of interstitial carbon on the γ-surface in austenite, Acta Mater. 61 (1) (2013) 341–349. doi:10.1016/j.actamat.2012.09.066.
URL https://www.sciencedirect.com/science/article/pii/S1359645412006994

[28] J. Cai, F. Wang, C. Lu, Y. Y. Wang, Structure and stacking-fault energy in metals Al, Pd, Pt, Ir, and Rh, Phys. Rev. B 69 (22) (2004) 224104. doi:10.1103/PhysRevB.69.224104.
URL https://link.aps.org/doi/10.1103/PhysRevB.69.224104

[29] X. Guo, Y. Xia, Repulsive force vs. source number: Competing mechanisms in the yield of twinned gold nanowires of finite length, Acta Mater. 59 (6) (2011) 2350–2357. doi:10.1016/j.actamat.2010.12.031.
URL https://www.sciencedirect.com/science/article/pii/S1359645410008633

[30] H. Y. Song, Y. Sun, Effect of coherent twin boundary and stacking fault on deformation behaviors of copper nanowires, Comput. Mater. Sci. 104 (2015) 46–51. doi:10.1016/j.commatsci.2015.03.052.
URL https://www.sciencedirect.com/science/article/pii/S0927025615002256

[31] J. D. Honeycutt, H. C. Andersen, Molecular dynamics study of melting and freezing of small Lennard-Jones clusters, J. Phys. Chem. 91 (19) (1987) 4950–4963. doi:10.1021/j100303a014.
URL https://doi.org/10.1021/j100303a014

[32] D. Faken, H. Jónsson, Systematic analysis of local atomic structure combined with 3D computer graphics, Comput. Mater. Sci. 2 (2) (1994) 279–286. doi:10.1016/0927-0256(94)90109-0.
URL https://www.sciencedirect.com/science/article/pii/0927025694901090

[33] S. Plimpton, Fast parallel algorithms for short-range molecular dynamics, J. Comput. Phys. 117 (1995) 1–19. doi:10.1006/jcph.1995.1039.
URL https://www.sciencedirect.com/science/article/pii/S002199918571039X

[34] S. M. Foiles, M. I. Baskes, M. S. Daw, Embedded-atom-method functions for the fcc metals Cu, Ag, Au, Ni, Pd, Pt, and their alloys, Phys. Rev. B 33 (1986) 7983–7991. doi:10.1103/PhysRevB.33.7983.
URL https://link.aps.org/doi/10.1103/PhysRevB.33.7983

[35] G. Grochola, S. P. Russo, I. K. Snook, On fitting a gold embedded atom method potential using the force matching method, J. Chem. Phys. 123 (20) (2005) 204719. doi:10.1063/1.2124667.

URL https://aip.scitation.org/doi/abs/10.1063/1.2124667

[36] M. I. Baskes, Modified embedded-atom potentials for cubic materials and impurities, Phys. Rev. B 46 (5) (1992) 2727–2742. doi:10.1103/PhysRevB.46.2727.
URL https://link.aps.org/doi/10.1103/PhysRevB.46.2727

[37] B.-J. Lee, J.-H. Shim, M. I. Baskes, Semiempirical atomic potentials for the fcc metals Cu, Ag, Au, Ni, Pd, Pt, Al, and Pb based on first and second nearest-neighbor modified embedded atom method, Phys. Rev. B 68 (14) (2003) 144112. doi:10.1103/PhysRevB.68.144112.
URL https://link.aps.org/doi/10.1103/PhysRevB.68.144112

[38] U. Wolf, P. Gumbsch, H. Ichinose, H. F. Fischmeister, Incoherent $\sum$ 3 grain boundaries in fcc metals : the influence of inclinaison on the boundary structure and energy, J. Phys. Colloq. 51 (1990) C1–366. doi:10.1051/jphyscol:1990157.
URL http://dx.doi.org/10.1051/jphyscol:1990157

[39] Y. F. Woguem, P. Godard, J. Durinck, S. Brochard, Atomic scale simulations of {112} symmetric incoherent twin boundaries in gold, Mater. 27 (2023) 101678. doi:10.1016/j.mtla.2023.101678.
URL https://www.sciencedirect.com/science/article/pii/S2589152923000066

[40] A. Stukowski, Visualization and analysis of atomistic simulation data with OVITO–the open visualization tool, Model. Simul. Mater. Sci. Eng. 18 (2009) 015012. doi:10.1088/0965-0393/18/1/015012.
URL https://doi.org/10.1088/0965-0393/18/1/015012

[41] T. J. Balk, K. J. Hemker, High resolution transmission electron microscopy of dislocation core dissociations in gold and iridium, Philos. Mag. A 81 (2001) 1507–1531. doi:10.1080/01418610108214360.
URL https://doi.org/10.1080/01418610108214360

[42] O. Nial, A. Almin, A. Westgren, Rontgenanalyse der systeme gold-antimon und silber-zinn, Z. Phys. Chem. 14B (1) (1931) 81–90. doi:10.1515/zpch-1931-1409.
URL https://www.degruyter.com/document/doi/10.1515/zpch-1931-1409/html

[43] J. R. Neighbours, G. A. Alers, Phys. Rev. 111 (3) (1958) 707–712. doi:10.1103/PhysRev.111.707, [link].
URL https://link.aps.org/doi/10.1103/PhysRev.111.707

[44] C. Deng, F. Sansoz, Fundamental differences in the plasticity of periodically twinned nanowires in Au, Ag, Al, Cu, Pb and Ni, Acta Mater. 57 (20) (2009) 6090–6101. doi:10.1016/j.actamat.2009.08.035.
URL https://www.sciencedirect.com/science/article/pii/S1359645409005473

[45] C. Deng, F. Sansoz, Size-dependent yield stress in twinned gold nanowires mediated by site-specific surface dislocation emission, Appl. Phys. Lett. 95 (9) (2009) 091914. doi:10.1063/1.3222936.
URL https://doi.org/10.1063/1.3222936

[46] S. M. A. A. Alvi, A. Faiyad, M. A. M. Munshi, M. Motalab, M. M. Islam, S. Saha, Cyclic and tensile deformations of gold–silver core shell systems using newly parameterized MEAM potential, Mech. Mater. 169 (2022) 104304. doi:10.1016/j.mechmat.2022.104304.
URL https://www.sciencedirect.com/science/article/pii/S0167663622000850

[47] C. L. Jia, A. Thust, Investigation of atomic displacements at a $\mathit{\ensuremath{\Sigma}}3$ {111} twin boundary in ${\mathrm{BaTiO}}_{3}$ by means of phase-retrieval electron microscopy, Phys. Rev. Lett. 82 (25) (1999) 5052–5055. doi:10.1103/PhysRevLett.82.5052.
URL https://link.aps.org/doi/10.1103/PhysRevLett.82.5052

[48] X. Ke, J. Ye, Z. Pan, J. Geng, M. F. Besser, D. Qu, A. Caro, J. Marian, R. T. Ott, Y. M. Wang, F. Sansoz, Ideal maximum strengths and defect-induced softening in nanocrystalline-nanotwinned metals, Nat. Mater. 18 (11) (2019) 1207–1214. doi:10.1038/s41563-019-0484-3.
URL https://www.nature.com/articles/s41563-019-0484-3

[49] S. Oh, M. Legros, D. Kiener, P. Gruber, G. Dehm, In situ tem straining of single crystal au films on polyimide: Change of deformation mechanisms at the nanoscale, Acta Mater. 55 (16) (2007) 5558–5571. doi:10.1016/j.actamat.2007.06.015.
URL https://linkinghub.elsevier.com/retrieve/pii/S1359645407004181

[50] J. Drieu La Rochelle, P. Godard, C. Mocuta, D. Thiaudière, J. Nicolai, M. F. Beaufort, M. Drouet, P. O. Renault, Study of uniaxial deformation behavior of 50 nm-thick thin film of gold single crystal using in situ X-ray pole figure measurements, Surf. Coat. Technol. 377 (2019) 124878. doi:10.1016/j.surfcoat.2019.06.103.
URL https://www.sciencedirect.com/science/article/pii/S0257897219308424

[51] X.-M. Luo, X.-F. Zhu, G.-P. Zhang, Nanotwin-assisted grain growth in nanocrystalline gold films under cyclic loading, Nat. Commun. 5 (1) (2014) 3021. doi:10.1038/ncomms4021.
URL https://www.nature.com/articles/ncomms4021